Extending the Characterization Bandwidth of Dynamic Nonlinear Transmitters with Application to Digital Predistortion

Souheil Bensmida, *Member, IEEE*, Oualid Hammi, *Member, IEEE*, Andrew Kwan, *Graduate Student Member, IEEE,* Mohammad S. Sharawi, *Senior Member*, IEEE, Kevin A. Morris, *Member, IEEE,* Fadhel M. Ghannouchi, *Fellow, IEEE*

***Abstract*— This paper reports a new measurement method for wideband radiofrequency power amplifier characterization and digital predistortion. The proposed measurement procedure relaxes significantly the sampling rate requirement on the analog to digital converters of the feedback path. Successful PA linearizations were achieved in the presence of 20 MHz, 40 MHz, and 60 MHz LTE-A signals using a vector signal analyzer with sampling speeds equal to only 24 Msps, 40.96 Msps, and 61.44 Msps, respectively. Despite these very low sampling rates, a quasi perfect cancellation of the PA distortions was achieved (more than 50 dBc in terms of ACLR), in all tests, over bandwidths including up to fifth order intermodulation distortions. Such correction bandwidth is much wider than the observation bandwidths associated with the receiver sampling rates.**

***Index Terms*—Digital predistortion, dynamic distortions, LTE-advanced, memory effects, power amplifier, vector signal analysis, wideband.**

I. Introduction

MODERN and future wireless communication systems provide high data rate capability. For this reason, transmitter architectures evolved to accommodate complex modulation schemes with high spectral efficiency. These architectures are designed to ensure the transmission of wideband signals in a linear manner. Any nonlinear behavior in the transmitter will distort the transmitted signal and hence corrupt the transmitted data. Radio frequency power amplifiers (RFPAs) are the most nonlinear and power consuming blocks in a transmitter's architecture. Therefore, special measures are taken to increase an RFPA linearity and efficiency. Significant research efforts have led to highly efficient RFPA architectures [1]-[7]. These architectures require linearization procedures to ensure compliance with the mandatory and well regulated linearity requirements of RFPAs.

Digital predistortion (DPD) is one of the most used linearization methods for cancelling out RFPAs nonlinear behavior [8][11][21]. DPD requires the characterization of RFPAs by analyzing their output signal over a certain bandwidth. This bandwidth value is typically five times the input signal bandwidth. Therefore, in order to implement an effective DPD, the feedback path used to demodulate the PA output signal requires a baseband sampling rate several times faster than the actual original baseband signal to be transmitted. For example, in modern wireless communication systems, the required sampling speed of the feedback path receiver is expected to be in the range of 500 Msps for 100 MHz wide LTE-Advanced signals.

In a research and development laboratory environment, power amplifiers distortions are characterized using modulated test signals. This requires the use of an arbitrary waveform generator (AWG) to feed the amplifier with the RF test signal and a vector signal analyzer (VSA) to demodulate the amplifier's output signal. Only expensive VSAs might be able to offer the measurement capabilities required by LTE and LTE-A signals. Moreover, in several cases, the available instruments cannot meet the sampling rate and dynamic range needed for PA linearization applications. In addition to instrument based PA characterization and predistortion test benches, a wide range of platforms was reported in the literature as summarized in [12]. Among others, dedicated self-developed PA characterization and digital predistortion platforms using in-house designed signal generators and receivers were reported [13][14]. In this case also, the sampling rate limitation of the feedback path is a serious challenge that needs to be addressed. Thus, it is essential to

Manuscript submitted January 13, 2015, re-submitted July 27, 2015, revised December 5, 2015, revised February 7, 2016, revised June 21, 2016. This work was supported by the University of Bristol and King Fahd University of Petroleum and Minerals (KFUPM). The work of the iRadio Laboratory was supported mainly by Alberta Innovates - Technology Futures (AITF), Canada Research Chair (CRC) Program, and Natural Science and Engineering Council of Canada (NSERC).

S. Bensmida and K.A. Morris are with are with the Communications Systems and Networks Group, University of Bristol, Bristol BS8 1UB, U.K. (e-mail: {s.bensmida, Kevin.Morris}@bristol.ac.uk).

O. Hammi is with the Department of Electrical Engineering, American University of Sharjah, Sharjah, United Arab Emirates (e-mail: ohammi@ieee.org)

A. Kwan and F.M. Ghannouchi are with the iRadio Laboratory, Department of Electrical and Computer Engineering, Schulich School of Engineering, University of Calgary, Calgary, AB T2N 1N4, Canada (e-mail: {akckwan, fadhel.ghannouchi}@ucalgary.ca).

M.S. Sharawi is with the Department of Electrical Engineering, King Fahd University of Petroleum and Minerals, Dhahran 31261, Saudi Arabia (e-mail: msharawi@kfupm.edu.sa).

come up with experimental procedures that would allow for the extension of the observation bandwidth of vector signal analysis test and measurement equipment in particular, and the feedback path of experimental digital predistortion systems in general. To address this, several signal acquisition techniques have been reported in the literature for various applications. Subsampling techniques were widely used in the presence of periodic signals with a relatively short time period value [15], as well as complex modulated signals [16]. In the case of modulated signals, the use of under-sampling techniques requires spacing between the different carriers in order to avoid spectrum overlap. Accordingly, it was successfully applied for dual band applications [16]. Though, it is not suitable for wideband systems involving contiguous carrier aggregation. The frequency stitching technique proposed by Wissel *et al.* in [17] provides wideband PA characterization by manipulating measurement data in the frequency domain leading to relatively complex signal processing. Other approaches have been proposed to extend the bandwidth of digital predistortion systems [18]-[21]. These include the band-limited Volterra series based digital predistortion approach in which the PA's and predistorter's outputs are filtered to reduce the sampling rate requirements [18]. In this prior work, it was demonstrated that the band-limited Volterra series approach outperforms conventional DPD systems operating at the same sampling rate. Though, a major limitation is that the correction bandwidth of this technique is equal to its observation bandwidth in the sense that the band limited DPD is unable to compensate for PA distortions outside the observation bandwidth. Recently, digital predistortion architectures with a correction bandwidth that exceeds the observation bandwidth have been reported. In [19], a spectral extrapolation technique was proposed to extend the correction bandwidth of DPD by means of computationally intensive signal processing algorithms. In [20], an under-sampling restoration DPD (USR-DPD) was introduced. The USR-DPD uses an iterative approach to synthesize the predistortion function. Its ability to significantly reduce the required sampling rate in the feedback path was found to be conditional to the presence of an analog band-pass filter in the feedback path. Without such filter, distortion mitigation beyond the observation bandwidth is compromised. Moreover, the USR-DPD requires an iterative process which might be perceived as a drawback in modern communication systems where fast adaptation is required. Authors in [21] proposed a sequential two-step synthesis of a two-box digital predistorter that considerably reduces the required sampling rate in the feedback path. However, this technique is suitable for a specific type of digital predistortion functions which are built using a two-box structure made of the cascade of a first dynamic predistortion function followed by a memoryless one. Even though these latter results are of great interest to the case of LTE-A power amplifiers, there is a need for other alternative techniques for broadband behavioral modeling and digital predistortion using low speed analog to digital converters.

In this work, we propose an original measurement procedure that relaxes the sampling speed requirement for VSAs in order to characterize and linearize RFPAs driven by broadband test signals as required for current and future wireless communication systems. The proposed measurement procedure is inspired from the under-sampling and time multiplexing techniques and is based on manipulating the test signals in the time-domain to extend the observation and thus the correction bandwidth of the feedback path without increasing the analog to digital converters' sampling speed. The use of a synthetic signal during the characterization step enables wideband linearization capability for experimental setups. Though, it prevents the use of the proposed technique in field deployed systems where the input signal manipulation needed to build the synthetic test signal is not feasible. The proposed technique is labeled MR-DAD for multiplexing based reconstruction of delayed, appended and down-sampled waveforms. Experiment results demonstrate the ability of the proposed technique in virtually increasing the vector signal analysis bandwidth of instrumentation systems and enabling a significant increase in the correction bandwidth of digital predistortion test beds. The remainder of this paper is organized as follows. The concept of the proposed approach and its theoretical background are discussed in Section II and Section III, respectively. The experimental validation of the proposed technique is reported in Section IV. The conclusions are presented in Section V.

II. Time Multiplexing Based Characterization Approach

A. Overview of the Proposed MR-DAD Technique

The main objective of this work is to develop a characterization technique that can allow for extending the observation bandwidth of vector signal analyzers without having to increase their sampling speed. It is worthy to note that, herein, vector signal analyzers are used to refer without loss of generality to the receiver used in the device under test (DUT) characterization experimental test bed.

The proposed MR-DAD technique is implemented to virtually increase the speed of currently available VSAs, thus extending the life cycle of test and measurement equipment, and reducing the cost of experimental setups. However, the adoption of the proposed technique is conditional to the availability of suitable system architecture where under-sampling induced aliasing effects are not prevented through the use band-limiting filters. In a PA characterization context, the testing signal is known and remains constant in terms of its statistics. This results in a stable PA response [17]. Exploiting this characteristic of PAs, the proposed technique is based on generating several copies of the input signal, and concatenating them with appropriate delay in order to result in a synthetic test signal. This synthetic test signal has the same characteristics (including statistics and bandwidth) as the original test signal. Thus, it will not have any noticeable impact on the power amplifier's behavior. The synthetic test signal is built using N (where N is an integer) versions of the original input signal each of these versions is generated by

delaying and wrapping the original input signal waveform. The synthetic baseband waveform is then used to generate the RF signal that will drive the device under test. At the receiver side, the acquisition of the power amplifier output waveform is performed at a low speed that is function of the number (N) of copies of the original waveform used to build the synthetic test signal. This approach allows for decreasing the sampling rate required at the receiver by a factor of N without compromising its accuracy, as shown in the remainder of the paper.

According to the description above, the proposed technique adapts and employs the under-sampling concept to the case of contiguous spectrums. Under-sampling ADCs have been used to reduce the sampling rate requirement in the feedback path of PA characterization and predistortion systems [16][22]. However, under-sampling a signal implies that frequency components from high order Nyquist zones will be folded back into the first Nyquist zone. The overlap between the frequency components coming from various Nyquist zones compromises the quality of the under-sampled signal and introduces errors between the reconstructed high speed signal and its original version. Thus, the use of under-sampling was limited to multi-band and widely spaced non-contiguous carriers in which it is possible to avoid the overlap between the aliased frequency components. Conversely, in this work, digital signal pre- and post-processing is adopted in order to enable the use of under-sampling techniques in signals having contiguous spectrum. The aliasing due to the under-sampling is recovered through appropriate multiplexing of the low speed sampled signal. In fact, multiplexing is commonly used in interleaved ADCs in order to reconstruct a high speed signal from a plurality of under-sampled versions of the same signal. However, it is important to distinguish here between interleaved ADC techniques in which a plurality of ADCs operating at low speed are used to sample a single signal waveform with a controlled delay between the ADCs, and the proposed technique in which a single ADC operating at low speed is used to sample multiple copies of a signal waveform delayed in such a way that it emulates the acquisition of interleaved ADCs. The advantages of the proposed technique over interleaved ADCs are twofold. First, in order to reduce the sampling rate by a factor N, it requires only a single ADC in contrast with N ADCs in the case of interleaved ADCs. Moreover, the use of interleaved ADCs requires tedious calibrations as described in [23], and a perfect time alignment in order to precisely reconstruct the high speed version of the under-sampled signal following the multiplexing step. Conversely, in the proposed approach, the signal is pre- and post-processed in the digital domain in order to ensure a perfect reconstruction of the high speed waveform following the multiplexing step.

A block diagram of the proposed digital predistortion system is presented in Fig. 1. The original signal $(x(n))$ is generated by the signal source, and then pre-processed by a digital signal processing module to build the corresponding test signal $(x_{syn}(n))$. The detailed description of the signal pre-processing module functionality is provided below along with the equations relating the signals $x(n)$ and $x_{syn}(n)$. The digital waveform at the output of the signal pre-processing module is then fed into a vector signal generator which will drive the device under test with the corresponding RF analog signal. The signal at the output of the device under test is under-sampled by the vector signal analyzer. Finally, the resulting digital waveform $(y_{LS}(n))$ at the output of the VSA is properly multiplexed by the signal post-processing unit in order to obtain the reconstructed signal $(y_{rec}(n))$ that will be used along with the input signal $(x(n))$ to derive the DUT's behavioral model and or synthesize the digital predistortion function.

B. Detailed Description for N=2

Fig. 2 depicts a graphical illustration of the signals involved in the proposed technique for $N=2$. The original waveform is initially sampled at a rate f_S. A second copy of the original signal is appended to a first copy of the original waveform after applying a one sample delay to the second one. Accordingly, sampling the resulting synthetic signal at a rate of $f_S/2$ will result in the acquisition of the samples having originally odd indices from the signal's first copy and the samples having originally even indices from the signal's second copy. Thus, all required samples are acquired but not in sequence. To circumvent this issue, a multiplexing of the samples acquired from the first and the second copies of the original signal is performed as illustrated in Fig. 2. At the end of this step, the reconstructed signal built from sampling, at a rate of $f_S/2$, the output signal obtained by applying the synthetic input signal is ideally identical to that obtained by sampling at a rate of f_S the PA's output signal corresponding to the original input signal. Practically, some measurement errors will be present due to the fact that unavoidable noise measurement is obtained when the same signal is acquired several times. The impact of these measurement errors on the performance of the proposed technique is investigated in the next section. It is worth mentioning here that the synthetic test signal does not induce any noticeable time-domain discontinuity. In fact, the signal waveforms commonly used in PAs characterization experiments have limited length (typically few ms), and are played repeatedly by the signal generator during the characterization / linearization tests. Thus, these test signals are inherently continuous. In the proposed technique, a one sample delay is introduced between a segment of the waveform and the next one. As such, a one sample delay would not introduce any noticeable effect on the signal's time-domain continuity and thus its bandwidth.

It is worth noting that the very high degree of similarity between the baseband waveforms of the original and the synthetic signals ensures a quasi identical behavior of the

DUT including its static and dynamic distortions. This is expected to lead to quasi perfect cancellation of the PA distortion when a digital predistortion function will be built using the synthetic test signal rather than the original signal.

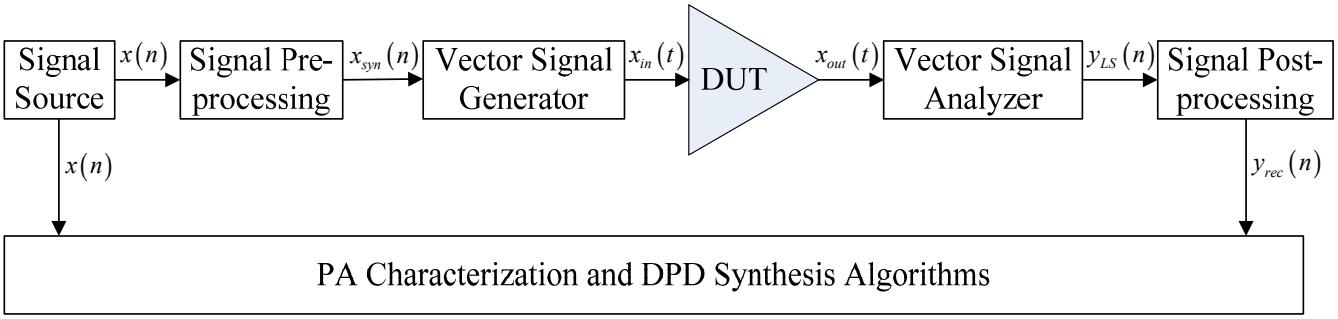

Fig. 1. Block diagram of the proposed digital predistortion system.

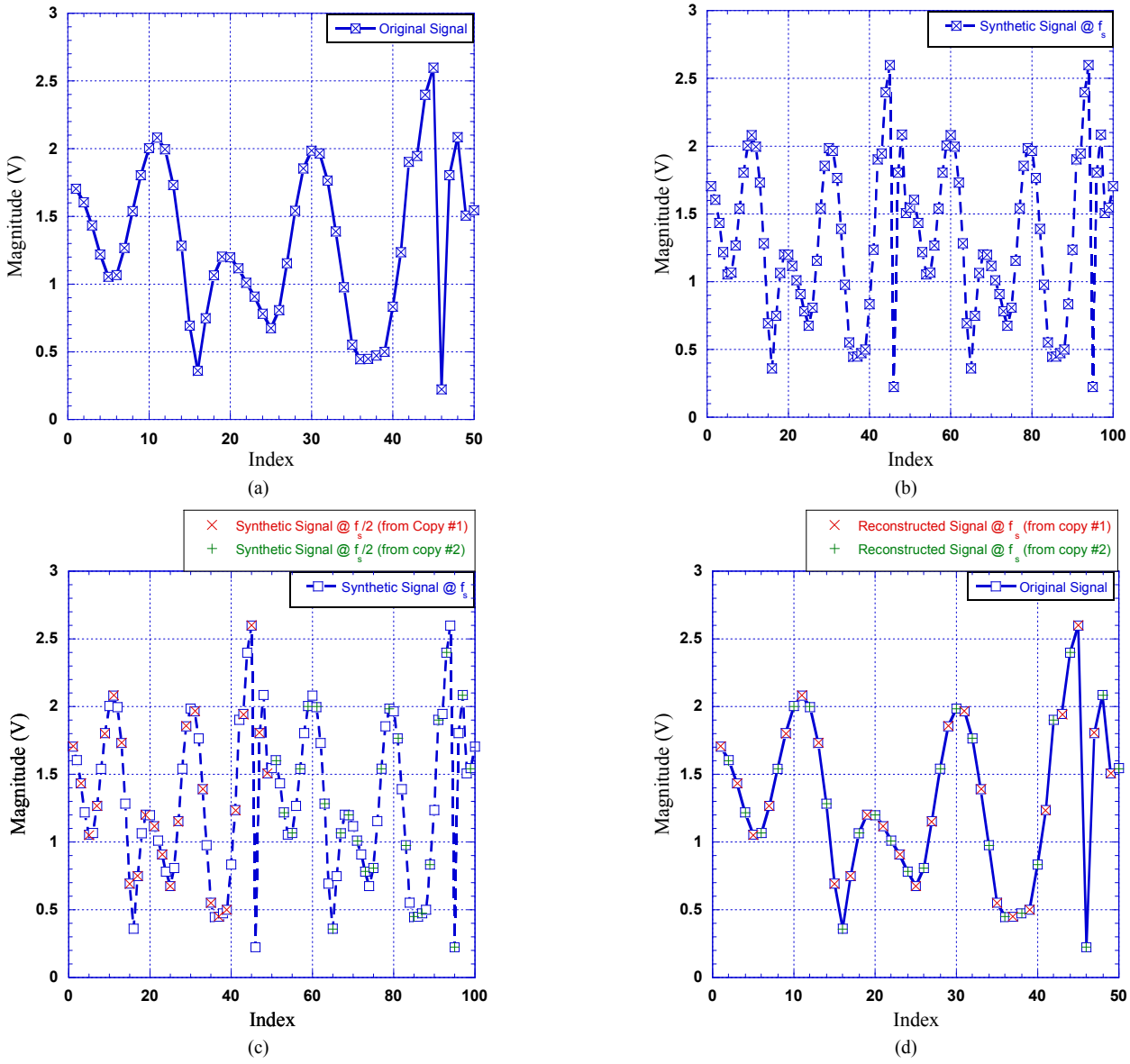

Fig. 2. Concept of synthetic test signal generation $(N=2)$. (a) Original input waveform. (b) Synthetic input waveform, (c) Output samples at low speed, (d) Final output (after multiplexing).

To better illustrate the proposed technique, let's consider the numerical example of a signal waveform having $K = 6$ samples. The original waveform sampled at f_S is a $K \times 1$ vector given by

$$\mathbf{x} = \begin{bmatrix} x(1) & x(2) & x(3) & x(4) & x(5) & x(6) \end{bmatrix}. \quad (1)$$

For $N = 2$, the synthetic test signal sampled at f_S is an $NK \times 1$ vector:

$$\mathbf{x_{syn}} = \begin{bmatrix} x(1) & \cdots & x(6) & x(2) & \cdots & x(6) & x(1) \end{bmatrix}. \quad (2)$$

Accordingly, the under-sampled signal operating at f_S/N at the output of the PA (for $N = 2$), will be a $K \times 1$ vector in which the samples of the signal appear in the following sequence

$$\mathbf{y_{LS}} = \begin{bmatrix} y(1) & y(3) & y(5) & y(2) & y(4) & y(6) \end{bmatrix}. \quad (3)$$

Post-processing the under-sampled output signal by multiplexing the first three $(K/N = 3)$ samples and the last three samples leads to the reconstructed output signal ($K \times 1$ vector) given by:

$$\mathbf{y_{rec}} = \begin{bmatrix} y(1) & y(2) & y(3) & y(4) & y(5) & y(6) \end{bmatrix}. \quad (4)$$

C. Generalization to Arbitrary Value of N

The technique described above for the case of $N = 2$ can be generalized to any value of N provided that the signal length K is multiple of N as it will be shown through (9). Increasing the value of N will result in longer waveforms. However, memory limitations in the test measurements can be circumvented by reducing the length (K) of the original waveform to ensure that the length of the synthetic signal can be handled by the vector signal analyzer. The flow chart of the algorithm proposed for building the synthetic test signal and reconstructing the high speed output signal from the waveform measured at a lower speed is presented in Fig. 3. First, the value of N is selected. Then, the synthetic waveform is built by appending N copies of the original signal. A one sample delay is included between each copy of the signal and the preceding copy. The delayed samples are added at the end of the corresponding waveform copy. To better illustrate this key concept, let's consider the original input baseband waveform, x, that is given by:

$$x = \begin{bmatrix} x(1) & x(2) & \cdots & x(l-1) & x(l) & \cdots & x(K) \end{bmatrix}. \quad (5)$$

Then, the n^{th} copy of the input signal (for $n > 1$) will be

$$x_n = \begin{bmatrix} x(n) & x(n+1) & \cdots & x(K) & x(1) & \cdots & x(n-1) \end{bmatrix}. \quad (6)$$

The signals x_1 through x_N are then concatenated to build the synthetic input waveform x_{syn} according to

$$x_{syn} = \begin{bmatrix} x_1 & x_2 & \cdots & x_N \end{bmatrix}. \quad (7)$$

Next, the synthetic baseband waveform, x_{syn}, is used to generate the RF test signal to be applied at the input of the DUT. The output waveform of the device under test is acquired at a lower sampling rate, f_S/N, compared to the sampling rate, f_S, of the baseband input waveform. The resulting low speed (LS) baseband output waveform, y_{LS}, will be:

$$y_{LS} = \begin{bmatrix} y_{syn}(1) \\ y_{syn}(N+1) \\ y_{syn}(2N+1) \\ \vdots \\ y_{syn}(N(K-1)+1) \end{bmatrix}^T, \quad (8)$$

where $[\ ]^T$ denotes the matrix transpose operator, and y_{syn} corresponds to the baseband output waveform that would have been obtained if synchronous sampling rate of f_S was used in the vector signal analyzer to sample the output of the DUT driven by the synthetic baseband waveform, x_{syn}.

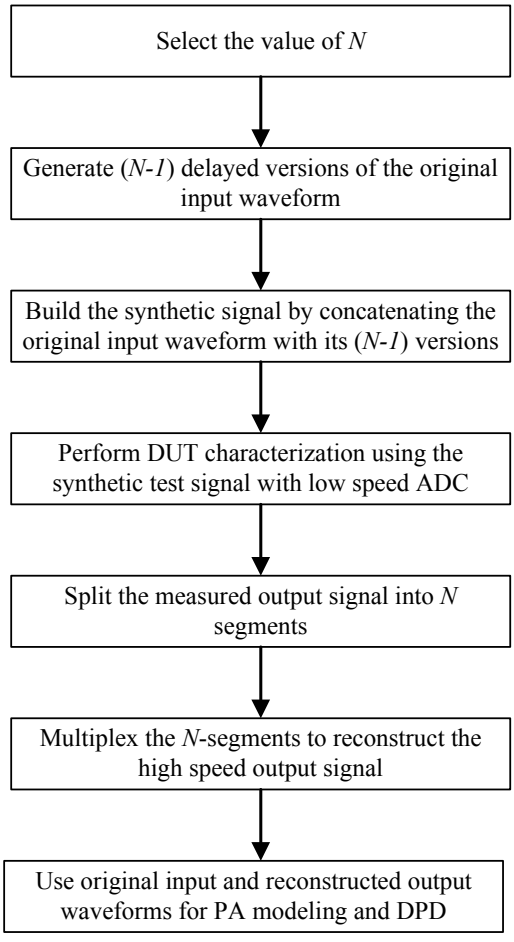

Fig. 3. Flow chart of the proposed characterization technique.

The baseband output waveform, y_{LS}, acquired at a low speed is then split into N signals of equal length given by:

TABLE I
CHARACTERISTICS OF THE WAVEFORMS USED IN THE CHARACTERIZATION PROCESS

Signal	Number of Samples	Sampling Rate (Hz)	Waveform Length (s)
Original input (x)	K	f_S	K/f_s
Synthetic input (x_{syn})	$N \cdot K$	f_S	$N \cdot \left(K/f_s\right)$
Synthetic output (y_{syn})	$N \cdot K$	f_S	$N \cdot \left(K/f_s\right)$
Acquired output (y_{LS})	K	f_s/N	$N \cdot \left(K/f_s\right)$
Reconstructed output (y_{rec})	K	f_S	K/f_s
Output using conventional approach (y)	K	f_S	K/f_s

$$y_{LS,n} = \begin{bmatrix} y_{LS}\left((n-1)\times\left(\frac{K}{N}\right)+1\right) \\ y_{LS}\left((n-1)\times\left(\frac{K}{N}\right)+2\right) \\ \vdots \\ y_{LS}\left(n\frac{K}{N}\right) \end{bmatrix}^T, \quad (9)$$

where n is an integer varying from 1 to N. (9) implies that the waveform length K is a multiple of N. This can be easily ensured in the experimental setup through appropriate selection of the length of the original baseband waveform x.

The signals $y_{LS,k}$ are then interleaved to construct the final version, y_{rec}, of the DUT's baseband output signal according to:

$$y_{rec} = \begin{bmatrix} y_{LS,1}(1) \\ y_{LS,2}(1) \\ \vdots \\ y_{LS,N}(1) \\ y_{LS,1}(2) \\ \vdots \\ y_{LS,N}\left(\frac{K}{N}\right) \end{bmatrix}^T. \quad (10)$$

The baseband output waveform, y_{rec}, is then used along with the original baseband input waveform, x, to perform time-delay alignment and then extract the PA behavioral model and / or digital predistortion function.

Table I summarizes the characteristics of the different waveforms involved in the proposed characterization technique. This includes the length in terms of number of samples as well as the sampling rate of each of these signals. According to this table, the value of N will have two direct impacts on the measurements. First, it will reduce the required sampling rate at the receiver from f_S to f_S/N. Second, it will increase the length, in terms of number of samples, of the baseband waveforms applied at the input of the DUT. In fact, if the original input waveform, x, sampled at a rate f_S includes K samples, then the synthetic waveform at the input of the DUT will have $N \times K$ samples at a rate of f_S. Conversely, the waveform acquired at the output of the DUT will have K samples only since it will be sampled at f_S/N.

The use of low speed analogue to digital converters (ADCs) at the receiver side is beneficial in terms of dynamic range capability and cost implementation. In addition to its key advantage resulting from extending the distortion characterization and mitigation bandwidths beyond the receiver observation bandwidth, the proposed method has the advantage of being reconfigurable in terms of required demodulation bandwidth for wideband PA characterization while benefiting from the high dynamic range of low speed ADCs.

III. THEORETICAL BACKGROUND AND PERFORMANCE ANALYSIS

In this section, a theoretical comparison between the acquisition of the DUT output using the conventional and the proposed MR-DAD approaches is carried out. In the conventional approach, the K samples long baseband output waveform y is acquired at a sampling rate of f_s. Conversely, in the proposed MR-DAD approach, the K samples baseband output waveform y_{rec}, sampled at f_s, is obtained by time multiplexing the N fragments, $y_{LS,k}$, of the baseband output waveform y_{LS} measured at a low sampling rate of f_s/N.

First, the analysis is performed for $N=2$, then it is generalized to an arbitrary value of N. In this case, by comparing the data acquired using the high speed and low speed approaches, it appears that the samples of odd indexes in the reconstructed waveform are identical to those acquired at the same instants with the conventional approach. Conversely, the samples of even indexes in the reconstructed and high speed waveforms are acquired at two different time instants. This is further clarified by (11).

Combining (10) and (9), leads to

$$\begin{cases} y_{rec}(k) = y_{LS,1}\left(\frac{k+1}{2}\right) = y_{LS}\left(\frac{k+1}{2}\right) & for\ k\ odd \\ y_{rec}(k) = y_{LS,2}\left(\frac{k}{2}\right) = y_{LS}\left(\frac{K+k}{2}\right) & for\ k\ even \end{cases}, \quad (11)$$

where k is an index that varies from 1 to K.

In order to assess the accuracy of the proposed characterization technique, it is useful to examine the difference between acquiring the DUT output signal using the

conventional approach and acquiring it using the proposed MR-DAD approach. In the conventional approach, the output signal is sampled at f_S to obtain the baseband waveform y. Conversely, in the MR-DAD approach, the output is sampled at $f_S/2$ to obtain the baseband waveform y_{LS}. This latter waveform is then digitally processed to build the reconstructed signal y_{rec}. Based on (8) and (11), it appears that odd order samples of both output waveforms (y and y_{rec}) are the same, while even order samples are acquired at two different instants. Thus, it is expected that even order samples of the output signals y and y_{rec} will not be perfectly identical. Accordingly,

$$\begin{cases} y_{rec}(k) = y_{syn}(k) = y(k) & for\ k\ odd \\ y_{rec}(k) = y_{syn}(K+k-1) = y(k)+\varepsilon(k) & for\ k\ even \end{cases}, \quad (12)$$

where k is an index that varies from 1 to K, and $\varepsilon(k)$ represents the measurement error for the k^{th} sample of the reconstructed output signal.

The discrete Fourier transform (DFT) of the output waveforms $y(k)$ and $y_{rec}(k)$ are, by definition, given by:

$$Y(f) = \sum_{k=1}^{K} y(k) e^{-j\frac{2\pi f}{K}k}, \quad (13)$$

and

$$Y_{rec}(f) = \sum_{k=1}^{K} y_{rec}(k) e^{-j\frac{2\pi f}{K}k}. \quad (14)$$

Transforming (12) in frequency domain using (14) gives:

$$Y_{rec}(f) = \left[\sum_{\substack{k=1 \\ k\ odd}}^{K-1} y(k) e^{-j\frac{2\pi f}{K}k}\right] + \left[\sum_{\substack{k=2 \\ k\ even}}^{K} \left[y(k)+\varepsilon(k)\right] e^{-j\frac{2\pi f}{K}k}\right]. \quad (15)$$

Rearranging (15) as follows:

$$Y_{rec}(f) = \left[\sum_{\substack{k=1 \\ k\ odd}}^{K-1} y(k) e^{-j\frac{2\pi f}{K}k}\right] + \left[\sum_{\substack{k=2 \\ k\ even}}^{K} y(k) e^{-j\frac{2\pi f}{K}k}\right] + \left[\sum_{\substack{k=2 \\ k\ even}}^{K} \varepsilon(k) e^{-j\frac{2\pi f}{K}k}\right]. \quad (16)$$

The relationship between the DFT of the original and the reconstructed output signals can then be written as:

$$Y_{rec}(f) = Y(f) + \left[\sum_{k=1}^{\frac{K}{2}} \varepsilon(2k) e^{-j\frac{2\pi f}{K}(2k)}\right]. \quad (17)$$

(17) describes the DFT of the reconstructed output baseband waveform with the proposed technique for $N=2$.

For any value of N, the generalized form of (17) can be written as:

$$Y_{rec}(f) = Y(f) + \sum_{n=2}^{N}\left[\sum_{m=1}^{\frac{K-N+n}{2}} \varepsilon_n(N\cdot m) e^{-j\frac{2\pi f}{K}(N\cdot m)}\right], \quad (18)$$

where ε_n is the measurement error vector corresponding to the n^{th} segment of the baseband output waveform ($y_{LS,n}$).

By evaluating then the last term of (18), it is possible to predict the effect that the proposed technique will have on the spectrum of the reconstructed signal. This can be done easily due to the fact that the error between the original signal and the reconstructed one is demonstrated to be a simple additive term given by:

$$\Delta Y_N(f) = \sum_{n=2}^{N}\left[\sum_{m=1}^{\frac{K-N+n}{2}} \varepsilon_n(N\cdot m) e^{-j\frac{2\pi f}{K}(N\cdot m)}\right]. \quad (19)$$

Fig. 4 shows ΔY_N versus frequency for several values of N. In this figure, ε_n had a normal distribution scaled to represent measurement errors. The impact of the proposed technique can be seen in specific frequency components that depend on the value of N. The reconstructed signal is likely to have, in addition to the original signal frequency components, the same predicted frequency components present in Fig. 4 which are due to the wrapping technique only. To confirm this, the wrapping is implemented with a MATLAB simulation for several values of N, and the DFT of the reconstructed signal is calculated. An LTE signal with a bandwidth of 20 MHz is used with the same error distribution ε_n. Fig. 5 shows the spectrum of the reconstructed signal exhibiting identical frequency components to the ones predicted by (19) in Fig. 4. It is clear then that the effect of the proposed technique on the reconstructed signal characteristics can be predicted and precisely calculated and is therefore easy to compensate for, if needed.

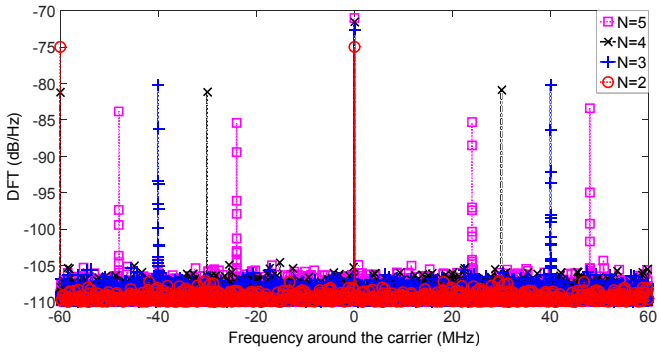

Fig. 4. Discrete Fourier Transform of ΔY_N for $N=2$, 3, 4, and 5.

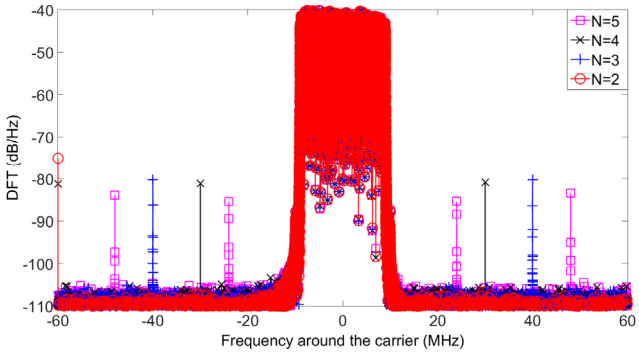

Fig. 5. Discrete Fourier Transform of the simulated reconstructed signal for $N = 2,\ 3,\ 4,$ and 5 .

In addition to the simulations, the proposed technique was implemented with a vector signal generator connected directly to a vector signal analyzer in order to investigate and confirm whether or not the predicted frequency components are present. Fig. 6 shows the spectrum of the reconstructed signal for several values of N and confirms what (19) predicts in terms of errors between the original signal and the reconstructed one. This is further demonstrated in Fig. 7 where the signal error due to the proposed technique is calculated, for $N = 5$, with (19) and as follows:

$$\Delta Y_N(f) = Y_{rec}(f) - Y(f). \tag{20}$$

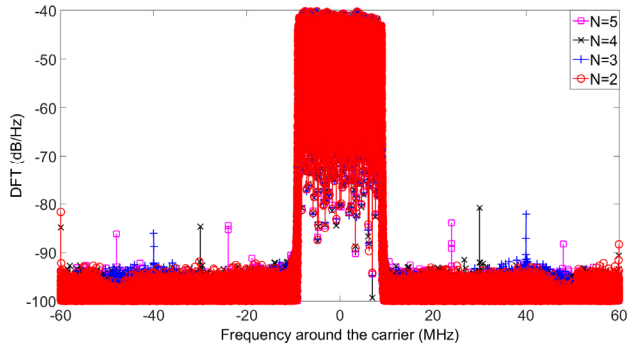

Fig. 6. Discrete Fourier Transform of the measured reconstructed signal for $N = 2,\ 3,\ 4,$ and 5 .

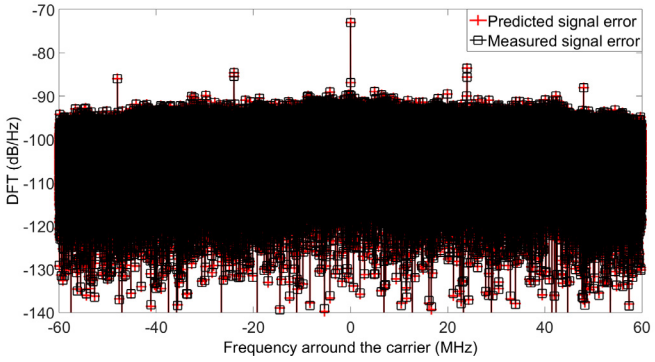

Fig. 7. Discrete Fourier Transform of the measured and predicted error signals for $N = 5$.

It is clearly shown in Fig. 6 that the prediction of the effect of the proposed technique is accurately achieved with (19).

At this stage, the effect of the wrapping technique has been assessed, formulated by (19), and calculated in the form of a signal error in the frequency domain. The reconstructed signal resemblance to the original signal is also assessed in the time domain using the normalized mean-squared error (NMSE) figure of merit. The calculated NMSE values that correspond to the cases where $N = 2,\ 3,\ 4,$ and 5 are -57 dB , -60 dB , -61 dB , and -61 dB , respectively. This level of NMSE shows that the effect of the proposed technique can be neglected and not compensated for without any significant impact on the characterization accuracy for both behavioral modeling and digital predistortion applications.

IV. Power Amplifier Linearization Using The Proposed Wrapping Technique

Two experimental setups were used to validate the proposed wrapping technique. Both setups are conceptually similar to the system block diagram of Fig. 1. In fact, for both cases, the signal source, signal pre- and post-processing as well as the PA characterization and DPD synthesis algorithms were implemented in software mainly using MATLAB. The vector signal generator and the vector signal analyzer used are commercial instruments. During the tests, a trigger signal is sent from the signal generator to initiate the data acquisition at the vector signal analyzer. K samples of the low speed signal, y_{LS} , are acquired by the VSA at a sampling rate of f_S/N .

It is important to recall that the performance of the proposed wrapping technique is conditional to having an anti-aliasing filter with a bandwidth wide enough in order not to filter any frequency component of the signal that will be under-sampled. This condition is indispensable for the perfect reconstruction of the signal in the post-processing step. However, most of the commercial instruments include band limited IF filters with bandwidths that are commensurate to the sampling rate of the ADC in order to avoid aliasing. In most of the cases, setting the sampling rate of the VSA will automatically select an IF filter that has narrower bandwidth than the sampling frequency entered in order to avoid aliasing. In these instruments, depending on the manufacturer, the ratio between the ADC sampling rate and the anti-aliasing filter bandwidth is equal to a pre-defined constant. In the first setup used in this work, the sampling rate of the VSA (model RS-FSQ-26 from Rohde and Schwarz) and the bandwidth of its anti-aliasing filter were "locked", in the sense that they cannot be independently controlled. Thus, the first test was performed to evaluate the potential of the proposed concept while performing the under-sampling in an artificial way by sampling the VSA input signal at a high speed and then deliberately sub-sampling the digital signal within the signal processing software. On the other hand, the VSA (model FSW26 signal and spectrum analyzer from Rohde and Schwarz) used in the second set of experiments allows for the

independent control of the sampling rate and the anti-aliasing filter bandwidth. In this case, it was possible to assess the performance of the proposed technique in a fully realistic context by setting the bandwidth of the anti-aliasing filter to its widest value while successively reducing the sampling rate to under-sample the test signal in the hardware. In the remainder of this section, the detailed description of the two experimental setups, the test conditions, and the results are presented.

The first test focused on validating the signal decomposition and reconstruction. A photograph of the setup used is depicted in Fig. 8. This setup includes a vector signal generator (VSG), SMATE200A from Rhode and Schwarz, followed by a high output power linear driver, the DUT and an output attenuator (10 dB) to accommodate the maximum power handling capabilities of the following vector signal analyzer (VSA), model RS-FSQ-26 from Rhode and Schwarz.

The PA architecture used in this first test is an inverse class-F PA operating at 900 MHz. A 20 MHz LTE signal was used to characterize this PA using a VSA sampling speed of 120 Msps, and a filter bandwidth of 160 MHz. This is referred to as the conventional approach in which a high enough sampling rate is adopted at the receiver to ensure the inclusion of all significant adjacent channels and thus optimal DPD performance. This conventional approach is used as a benchmark to evaluate the performances of the proposed MR-DAD technique. For this purpose, several tests were performed using the MR-DAD technique in which N was successively increased from 2 up to 5. Accordingly, in these tests, the sampling frequency of the VSA was reduced from 60 Msps for $N=2$ to 24 Msps for $N=5$. As mentioned above, the VSA used in this first test automatically adjusted the anti-aliasing IF filters bandwidths depending on the sampling rate which compromises the proposed approach. Therefore, to avoid this hardware limitation, the low sampling speeds quoted above were emulated by simply decimating the measurements sampled at 120 Msps.

In all the cases tested in the first set of experiments, the DPD is implemented using a memory polynomial structure having a memory depth of 3 and a nonlinearity order of 9. Fig. 9 reports the measured spectrum at the output of the linearized DUT using the conventional technique and the proposed technique with $N=5$. This figure clearly demonstrates the effectiveness of the proposed approach in perfectly linearizing the DUT even with an observation bandwidth that is as low as 1.2 times the bandwidth of the input signal. This evidently contrasts with common practice where the observation bandwidth is up to 5 times wider than the input signal bandwidth. Detailed results of the DPD performance as a function of the value of N are presented in Table II. This table shows that the linearization performance is independent of N, and that despite a significant decrease in the VSA sampling rate, the performance of the DPD remains similar to that obtained with a high speed sampling rate. Indeed, the proposed DPD approach maintains almost quasi-unchanged adjacent channel leakage ratios of -50.6 dBc and -52.3 dBc in the adjacent and the alternate adjacent channels, respectively. Moreover, an EVM of less than 1% is maintained. Assessing the success of the DPD synthesized with the proposed technique is the ultimate way to prove that the nonlinearities extraction, including memory effects, is accurate. Furthermore, the successful PA linearization obtained with the MR-DAD technique here is achieved without any compensation of the signal error that can be predicted by (19). This means that the used measurement setup (VSG and VSA) is capable of performing vector signal acquisition with a reliable level of repeatability which corroborates our assumption according to which the signal error associated with the proposed acquisition technique can be neglected. Moreover, the successful implementation of the DPD using the proposed approach clearly demonstrates the ability of the signal pre- and post-processing algorithms in compensating for the aliasing due to the under-sampling process, and reveals its effectiveness when signals having contiguous spectrum are handled.

TABLE II
INVERSE CLASS-F PA DPD PERFORMANCES

Configuration	ACLR (dBc)		Alternate ACLR (dBc)		Maximum EVM (%)
	left	Right	Left	Right	
Without DPD	32	33	50	50	8
DPD implemented using classic high speed vector signal analysis	50.6	50.4	52.5	52.2	≤ 1
DPD implemented using proposed technique with N=2	50.6	50.3	52.5	52	≤ 1
DPD implemented using proposed technique with N=3	50.8	50.6	52.5	52.3	≤ 1
DPD implemented using proposed technique with N=4	50.6	50.4	52.5	52.2	≤ 1
DPD implemented using proposed technique with N=5	50.6	50.6	52.5	52.2	≤ 1

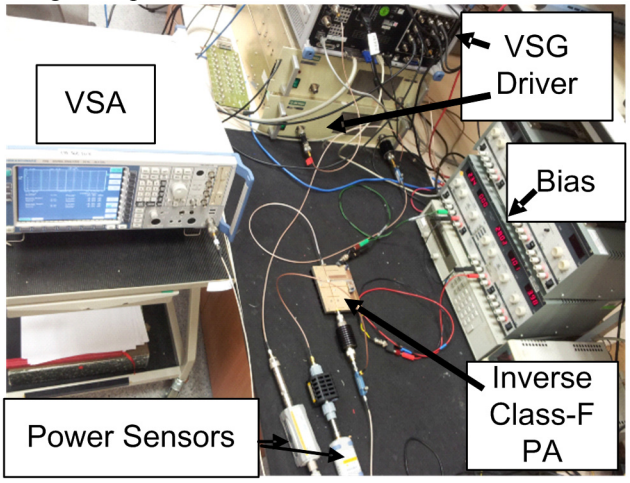

Fig. 8. Photograph of the first experimental setup with software implemented under-sampling.

The second set of measurements was performed using a different hardware set-up which provides more flexibility in the control of the anti-aliasing filter bandwidth. The VSG used is an Agilent 81180A arbitrary waveform generator connected to an Agilent E8267D for frequency up-conversion, and the VSA was a Rhode and Schwarz FSW26 Signal and Spectrum Analyzer. The VSA option used is R&S FSW-B320 which provides up to 320 MHz analysis bandwidth. In this VSA, it is possible to maintain the bandwidth of the anti-aliasing filter to its widest value while decreasing the sampling rate at which the ADCs will operate. This allows for the implementation of the under-sampling process within the hardware in contrast with the previous set of test where the under-sampling was emulated in the signal processing software. A photograph of this setup is reported in Fig. 10.

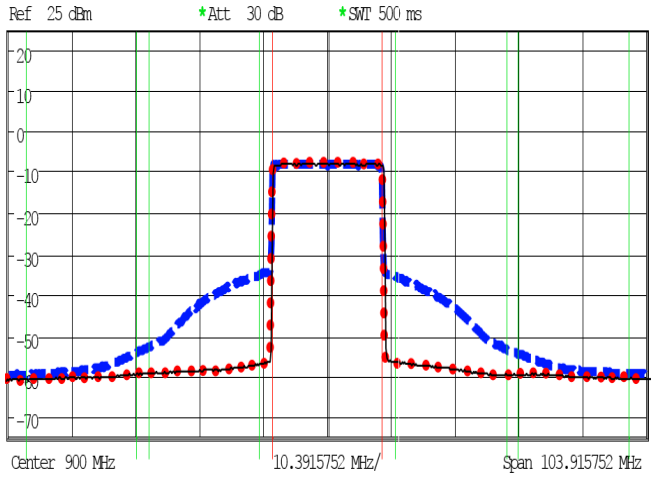

Fig. 9. Output signal spectrum of the first PA without DPD (blue dashes), with DPD based on classic measurement method (red dots), and with DPD based on the MR-DAD technique with N=5 (black solid line).

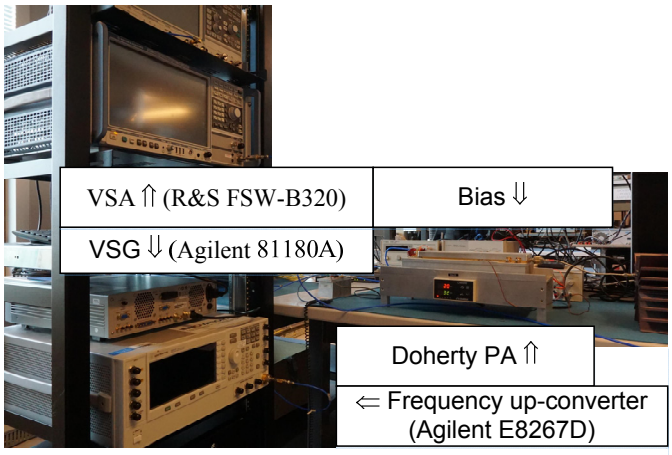

Fig. 10. Photograph of the second experimental setup with hardware implemented under-sampling.

The DUT used in this second test is a 300 Watt Doherty architecture based on LDMOS (laterally diffused MOSFET) devices. The test signal is an LTE-Advanced signal composed of two contiguous 20 MHz LTE signals centered at 2.14 GHz. To allow for a fine tuning of the sampling frequency during the test, the sampling frequency of the original signal was intentionally set to 368.64 Msps. In these experiments, the sampling frequency at the VSA was set to $\frac{368.64}{N}$ Msps , and N varied from 2 up to 9.

For each value of the VSA sampling rate, two DPDs were derived. The first was synthesized using the conventional approach where the input signal is the original one which does not include any appended delayed replicas. The second DPD was constructed using the proposed MR-DAD technique in which the under-sampling was implemented within the VSA hardware. In both approaches the DPD function was a memory polynomial having a nonlinearity order of 10 and a memory depth of 6. The measurement results are summarized in Fig. 11 which presents the measured ACLR in the lower and upper adjacent and alternate adjacent channels. From this figure, it appears that the conventional approach requires a minimum sampling rate of 92.16 Msps to meet the ACLR threshold of the LTE standard. However, as expected from the previous results, the MR-DAD based DPD technique maintains the distortion compensation even when a rate of 40.96 Msps is used to characterize the DUT driven by the 40 MHz LTE-A signal and synthesize its predistorter. Fig. 12 depicts the measured spectra at the output of the DUT as a function of the VSA sampling rate when the predistorter is built using each of the two approaches described above. Fig. 12 (a) illustrates the performance degradation as a function of the sampling rate in the case of the conventional approach. Conversely, Fig. 12 (b) demonstrates the robustness of the proposed approach when the sampling rate is decreased.

The second setup was also used to linearize the DUT when drive by a 3-carrier LTE-A signal having a total bandwidth of 60 MHz. A first DPD was built using the conventional approach in which the output signal was sampled at 368.64 Msps. A second DPD was constructed with the proposed method while sampling the output signal at only 61.44 Msps which corresponds to $N=6$. The spectra measured at the output of the linearized amplifier are reported in Fig. 13. This further confirms the performance of the proposed DPD and its ability to lead to same linearity as the conventional one while requiring significantly less sampling speed in the feedback path.

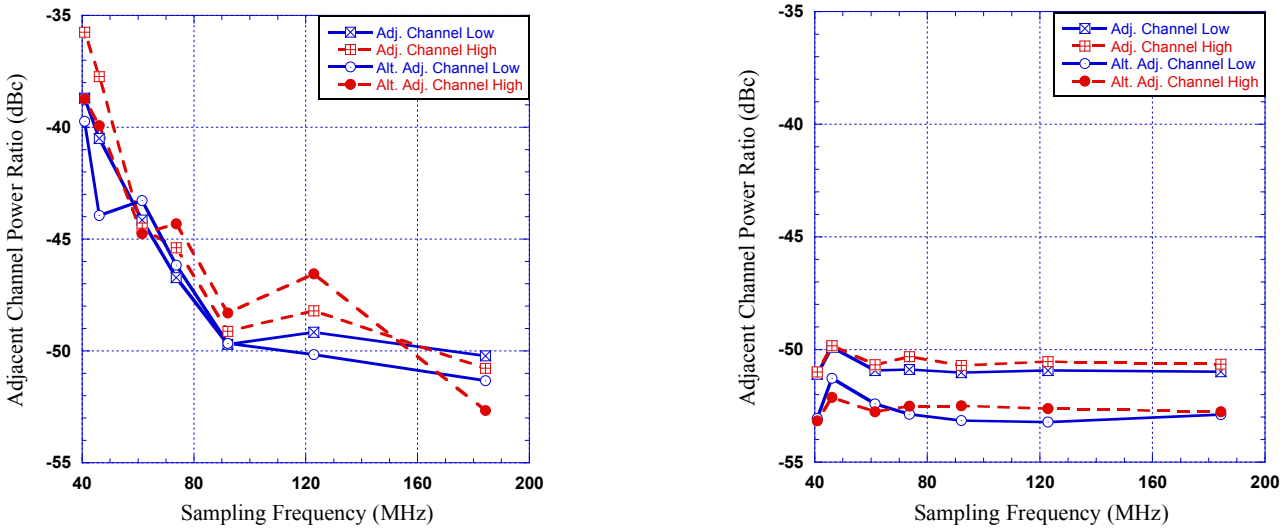

Fig. 11. ACLR at the output of the second PA as a function of the feedback ADC sampling rate measured with 40 MHz LTE-A input signal. (a) Conventional DPD. (b) Proposed MR-DAD DPD.

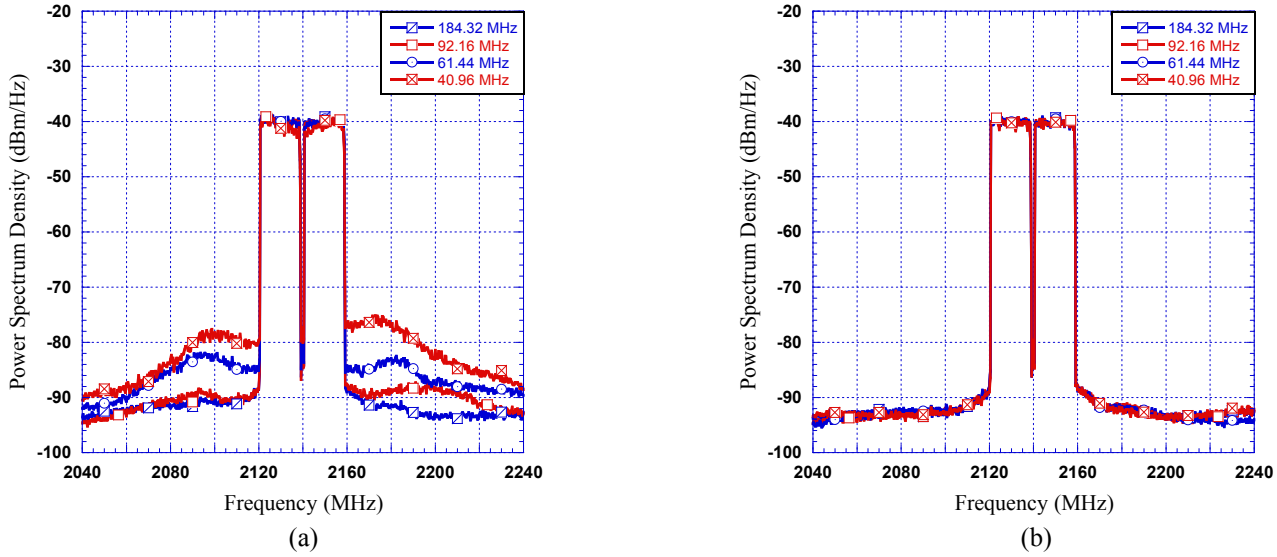

Fig. 12. Measured spectra at the output of the linearized PA as a function of the ADC sampling rate. (a) Conventional DPD, (b) Proposed DPD.

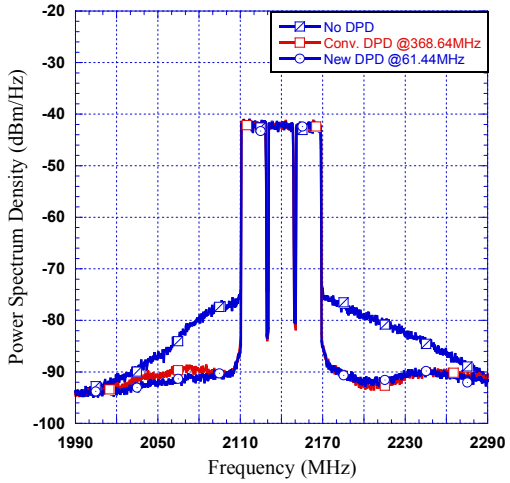

Fig. 13. Measured spectra at the output of the second DUT driven by 60MHz LTE-A signal.

V. Conclusions

In this paper, a novel characterization technique suitable for dynamic nonlinear power amplifiers driven by wideband test signals was proposed. This technique uses a synthetic test signal along with low complexity digital signal processing algorithm to reduce the sampling rate required at the receiver in order to accurately model the DUT. Experimental validation was carried using two power amplifiers prototypes driven by 20 MHz, 40 MHz, and 60 MHz wide LTE test signals. In all cases, it was shown that the proposed technique requires a sampling rate that is considerably lower than that of conventional DPD systems. Even though the use of the synthetic test signal makes this technique unsuitable for online use in field deployed systems, its advantages in a laboratory environment are highly competitive as it virtually extends the correction bandwidth of receivers by up to 5 times.

REFERENCES

[1] P. Wright, J. Lees, J. Benedikt, P.J. Tasker, and S.C. Cripps, "A methodology for realizing high efficiency class-J in a linear and broadband PA," *IEEE Trans. Microw. Theory Techn.,* vol. 57, no. 12, pp. 3196-3204, Dec. 2009.

[2] P.J. Tasker, V. Carrubba, P. Wright, J. Lees, J. Benedikt, and S. Cripps, "Wideband PA design: The "continuous" mode of operation," *IEEE Compound Semiconductor Integrated Circuit Symp. (CSICS)*, pp.1-4, Oct. 2012.

[3] K. Mimis, K.A. Morris, S. Bensmida, and J.P. McGeehan, "Multichannel and wideband power amplifier design methodology for 4G communication systems based on hybrid class-J operation," *IEEE Trans. Microw. Theory Techn.*, vol. 60, no. 8, pp. 2562-2570, Aug. 2012.

[4] M.N.A. Abadi, H. Golestaneh, H. Sarbishaei, and S. Boumaiza, "An extended bandwidth Doherty power amplifier using a novel output combiner," *IEEE MTT-S International Microw. Symp. (IMS2014)*, pp. 1-4, Jun. 2014.

[5] J. Lee, J. Son, and Bumman Kim, "Optimised Doherty power amplifier with auxiliary peaking cell," *Electron. Lett.*, vol. 50, no. 18, pp. 1299-1301, Aug. 2014

[6] T.M. Hone, S. Bensmida, K.A. Morris, M.A. Beach, J.P. McGeehan, J. Lees, J. Benedikt, and P.J. Tasker, "Inverse active load-pull in an inverse Doherty amplifier," *IEEE Topical Meeting on Power Amplifiers for Wireless and Radio Applications (PAWR 2013)*, pp. 4-6, Jan. 2013.

[7] A.M.M. Mohamed, S. Boumaiza, and R.R. Mansour, "Electronically tunable Doherty power amplifier for multi-mode multi-band base stations," *IEEE Trans. Circuits Syst. I, Reg. Papers,* vol. 61, no. 4, pp. 1229-1240, Apr. 2014.

[8] S. Bensmida, K. Mimis, K.A. Morris, M.A. Beach, J.P. McGeehan, J. Lees, J. Benedikt, and P.J Tasker, "Overlapped segment piece-wise polynomial pre-distortion for the linearisation of power amplifiers in the presence of high PAPR OFDM signals," *IEEE MTT-S International Microw. Symp. (IMS2012)*, pp. 1-3, Jun. 2012.

[9] O. Hammi, S. Bensmida, and K. Morris, "Behavioral modeling of class J amplifier driven by 100MHz LTE-advanced signal using dynamic nonlinearity reduction," *IEEE Topical Meeting on Power Amplifiers for Wireless and Radio Applications (PAWR 2014)*, pp. 67-69, Jan. 2014.

[10] L. Ding, G.T. Zhou, D.R. Morgan, Z. Ma, J.S. Kenney, J. Kim, and C.R. Giardina, "A robust digital baseband predistorter constructed using memory polynomials," *IEEE Trans. Commun.*, vol. 52, no. 1, pp. 159-165, Jan. 2004.

[11] S. Afsardoost, T. Eriksson, and C. Fager, "Digital predistortion using a vector-switched model," *IEEE Trans. Microw. Theory Techn.*, vol. 60, no. 4, pp. 1166-1174, Apr. 2012.

[12] L. Guan, and A. Zhu, "Green Communications," *IEEE Microw. Mag.*, vol. 15, no. 7, pp. 84-99, Nov. 2014.

[13] H.J. Wu, J. Xia, J.F. Zhai, L. Tian, M.S. Yang, L. Zhang, and X.W. Zhu, "A wideband digital pre-distortion platform with 100 MHz instantaneous bandwidth for LTE-advanced applications," *IEEE Workshop on Integrated Nonlinear Microwave and Millimetre-Wave Circuits (INMMIC 2012),* Dublin, Ireland, pp. 1-3, Sep. 2012.

[14] A. Kwan, O. Hammi, M. Helaoui, and F. M. Ghannouchi, "High performance wideband digital predistortion platform for 3G+ applications with better than 55dBc over 40 MHz bandwidth," *2010 IEEE MTT-S International Microwave Symposium (IMS 2010)*, Anaheim, CA, pp. 1082-1085, May 2010.

[15] H. Choi, A.V. Gomes, and A. Chatterjee, "Signal acquisition of high-speed periodic signals using incoherent sub-sampling and back-end signal reconstruction algorithms," *IEEE Trans. Very Large Scale Integr. (VLSI) Syst.*, vol. 19, no. 7, pp. 1125-1135, Jul. 2011.

[16] S.A. Bassam, A. Kwan, W. Chen, M. Helaoui, and F.M. Ghannouchi, "Subsampling feedback loop applicable to concurrent dual-band linearization architecture," *IEEE Trans. Microw. Theory Techn.*, vol. 60, no. 6, pp. 1990-1999, Jun. 2012.

[17] D. Wisell, D. Rönnow, and P. Händel, "A technique to extend the bandwidth of a power amplifier test-bed," *IEEE Trans. Instrum. Meas.*, vol. 56, no. 4, pp. 1488-1494, Aug. 2007.

[18] C. Yu, L. Guan, E. Zhu, and A. Zhu, "Band-limited Volterra series-based digital predistortion for wideband RF power amplifiers," *IEEE Trans. Microw. Theory Techn.*, vol. 60, no. 12, pp. 4198-4208, Dec. 2012.

[19] Y. Ma, Y. Yamao, Y. Akaiwa, and K. Ishibashi, "Wideband digital predistortion using spectral extrapolation of band-limited feedback signal," *IEEE Trans. Circuits Syst. I, Reg. Papers*, vol. 61, no. 7, pp. 2088-2097, Jul. 2014.

[20] Y. Liu, J.J. Yan, H.T. Dabag, and P.M. Asbeck, "Novel technique for wideband digital predistortion of power amplifiers with an under-sampling ADC," *IEEE Trans. Microw. Theory Techn.*, vol. 62, no. 11, pp. 2604-2617, Nov. 2014.

[21] O. Hammi, A. Kwan, S. Bensmida, K.A. Morris, and F.M. Ghannouchi, "A digital predistortion system with extended correction bandwidth with application to LTE-A nonlinear power amplifiers," *IEEE Trans. Circuits Syst. I, Reg. Papers*, vol. 61, no. 12, pp. 3487-3495, Dec. 2014.

[22] P. Cruz, N.B. Carvalho, "Modeling band-pass sampling receivers nonlinear behavior in different Nyquist zones," *IEEE MTT-S International Microw. Symp. (IMS2010)*, May 2010, pp.1684-1687.

[23] M. El-Chammas and B. Murmann, Background Calibration of Time-Interleaved Data Converters, Analog Circuits and Signal Processing, DOI 10.1007/978-1-4614-1511-4 2, © Springer Science+Business Media, LLC 2012.

Souheil Bensmida received the MSc. degree in electronics and instrumentation from the University of Pierre and Marie Curie Paris 6, Paris, France, in 2000, and the Ph.D. degree in electronics and communications from the Ecole Nationale Supérieure des Télécommunications (ENST), Paris, France, in 2005. Between October 2006 and August 2008, he was a Post-Doctoral Fellow with the iRadio Laboratory, University of Calgary, Canada. He is now Lecturer in Electrical and Electronic Engineering at University of Bristol, UK. His research interest is the non-linear characterisation and linearisation of power amplifiers for mobile and satellite applications and microwave instrumentation.

Oualid Hammi (S'03–M'09) received the B.Eng. degree from the École Nationale d'Ingénieurs de Tunis, Tunis, Tunisia, in 2001, the M.Sc. degree from the École Polytechnique de Montréal, Montréal, QC, Canada, in 2004, and the Ph.D. degree from the University of Calgary, Calgary, AB, Canada, in 2008, all in electrical engineering.

He is currently an Associate Professor with the Department of Electrical Engineering, American University of Sharjah, Sharjah, United Arab Emirates. He is also an Adjunct Professor with the Electrical and Computer Engineering Department, University of Calgary, Calgary, AB, Canada. From 2010 to 2015, he was a faculty member with the Department of Electrical Engineering, King Fahd University of Petroleum and Minerals, Dhahran, Saudi Arabia. From 2009 to 2010, he was a Post-Doctoral Fellow with the Intelligent RF Radio Laboratory (iRadio Lab), Schulich School of Engineering, University of Calgary. He has authored or co-authored one book, over 100 publications, and 11 US patents (including 5 pending). He is reviewer for several IEEE transactions. His research interests include the design of energy efficient linear transmitters for wireless communication systems and the characterization, behavioral modeling, and linearization of radiofrequency power amplifiers and transmitters.

Andrew Kwan (S'07) received his B.Sc. degree in computer engineering in 2006, M.Sc. degree in electrical engineering in 2009, and Ph.D. degree in electrical engineering in 2016 from the University of Calgary, Canada.

His research interests include signal processing for wireless communications systems, power efficiency enhancement for RF transceivers, embedded systems, and software defined radios.

Mohammad S. Sharawi (S'98–M'06–SM'10) received the Ph.D. degree in RF systems engineering from Oakland University, Oakland, MI, USA, in 2006. He is a Professor of electrical engineering at King Fahd University of Petroleum and Minerals (KFUPM), Dhahran, Saudi Arabia. He is the founder and director of the Antennas and Microwave Structure Design Laboratory (AMSDL). He obtained his Ph.D in RF Systems Engineering from Oakland University, Michigan, USA, in 2006. He was a visiting research Professor at the i-Radio Laboratory, University of Calgary, Alberta, Canada, for 6 months during 2014-2015. Dr. Sharawi was a Research Scientist with the Applied Electromagnetics and Wireless Laboratory, Oakland University, Michigan, USA, during the summer of 2013 and during 2008-2009. He was a faculty member in the Computer Engineering Department at the German-Jordanian and Philadelphia Universities, Amman, Jordan, during 2006-2008. During 2002-2003 he was a hardware design engineer with Silicon Graphics Inc., California, USA.

Dr. Sharawi has served on the technical and organizational committees of several international IEEE conferences especially EuCAP, APS, APWC, APCAP and ICCE. He has more than 150 refereed international journal and conference paper publications mostly in IEEE. Dr. Sharawi is the author of the Book "Printed MIMO Antenna Engineering," Artech House, 2014. He has authored/co-authored 6 book chapters in RF systems and antenna design. He was the recipient of the prestigious Excellence in Scientific Research award for the years 2014-2015, KFUPM. His research interests include Printed Multiple-input-multiple-output (MIMO) Antenna Systems, Miniaturized Printed Antennas and Antenna Arrays, Active Integrated Antennas, Reconfigurable Antennas, Microwave Circuits and Electronics, Millimeter-Wave Antennas and Antenna Arrays, and Applied Electromagnetics. He has 8 issued and 14 pending patents from the USPT O. Dr. Sharawi is a Senior Member IEEE, and Fellow IET.

Kevin A. Morris received his B.Eng. and Ph.D. degrees in electronics and communications engineering from the University of Bristol in 1995 and 1999 respectively. He currently holds the post of Reader in Radio Frequency Engineering within the Department of Electrical and Electronic Engineering at the University of Bristol. Currently he is involved with a number of research programmes within the U.K. He has authored or co-authored 60 academic papers and is the joint author of 5 patents. His research interests are principally in looking at methods of reducing power consumption in communications systems including the area of radio frequency hardware design with specific interest in the design of efficient linear broadband power amplifiers for use within future communications systems.

Fadhel Ghannouchi (S'84, M'88, SM'93, FIEEE' 07) is currently a professor and AITF/CRC Chair at Electrical and Computer Engineering Department of The Schulich School of Engineering of the University of Calgary and Director of Intelligent RF Radio Laboratory (www.iradio.ucalgary.ca). His research interests are in the areas of microwave instrumentation and measurements, nonlinear modeling of microwave devices and communications systems, design of power and spectrum efficient microwave amplification systems and design of intelligent RF transceivers for wireless and satellite communications. His research activities led to over 600 publications and 15 US patents (5 pending) and three books.